



Numerical Investigation on the three-Dimensional Flowfield in the Single Expansion Ramp Nozzle with Passive Cavity Flow Control

L. Zhou[†] and Z. Wang

Shaanxi Key Laboratory of Internal Aerodynamics in Aero-Engine, School of Power and Energy, Northwestern Polytechnical University, Xi'an, Shan Xi Province, 710072, China

[†]Corresponding Author Email: zhouli@nwpu.edu.cn

(Received June 27, 2018; accepted December 2, 2018)

ABSTRACT

Single Expansion Ramp Nozzle (SERN) with large expansion ratio is normally adopted for the hypersonic aircraft in consideration of integrated aircraft / propulsion system / nozzle design. Under low Mach number and low Nozzle Pressure Ratio (NPR, the ratio of inlet total pressure to outlet static pressure) conditions, the flow in the SERN is a state of severe over-expansion, the internal resistance increased obviously, the flow quality and performance of the SERN sharply deteriorated. How to effectively improve the SERN performance under over-expanded condition has become an important issue in the integrated design of hypersonic propulsion system. The passive cavity flow control technique was introduced on the upper expansion ramp of the SERN in this paper, the three-dimensional flowfield in the passive cavity SERN was investigated numerically, suitable NPR range for passive cavity flow control and impacts of passive cavity parameters were discussed. Results show the SERN performance is effectively improved when the passive cavity is applied from NPR of 5 to 10. Compared with the baseline SERN, 3.13 % improvement can be achieved for the thrust coefficient of the passive cavity SERN when NPR is 5. The passive cavity has the capacity of regulating the induced shock intensity or restraining flow separation, the reason for the change in its function is decided by the relative position between the induced shock and the passive cavity position on the upper expansion ramp of the SERN. As for each function of the passive cavity, an optimum position for the passive cavity structure exists on the upper expansion ramp. Among the primary geometric parameters of the passive cavity structure, percent of porosity is a crucial factor to affect the SERN performance by adjusting separation zone size and its separation starting position, and the improvement effectiveness of the axial thrust coefficient drops with the decrease of percent of porosity. The cavity depth and the aperture size are not sensitive to the performance of passive cavity SERN as compared to the effect of the percent of porosity.

Keywords: Single expansion ramp nozzle; Over-expanded condition; Passive cavity; Flow control technique; Geometric parameter.

NOMENCLATURE

A_l	the nozzle exit area	W_P	mass flow rate in SERN
A_r	area of single expansion ramp	V_x	axial velocity
$C_{f_{gx}}$	axial thrust coefficient	X_f	axial position of leading edge of the passive cavity
F_i	ideal thrust of SERN	X_b	axial position of trailing edge of the passive cavity
F_j	actual axial thrust of SERN		
L_r	axial length of the upper expansion ramp		
P	static pressure	ρ	density of the gas
P_j	total pressure	γ	specific heat ratio
P_∞	ambient pressure	Δ	change in property
R	gas constant		
T_j	total temperature		

1. INTRODUCTION

Exhaust nozzle is an important part for the air-breathing propulsion system. For the hypersonic aircraft with wide range of flight envelope (flight height is from 0 to 30 km or even higher altitude, Mach number changes from subsonic, transonic, supersonic to hypersonic condition), SERN is widely used in the design process in consideration of integrated aircraft / propulsion system / nozzle design (Deere and Asbury, 1999). The typical feature of SERN can be summarized as especially high design Mach number, high NPR, very broad operation scope (flight Mach number and flight height) and obvious asymmetrical geometric feature. The flow in the SERN is sensitive to the change of the external parameters. Under low Mach number and low NPR conditions, the flow in the SERN is a state of severe over-expansion, the internal resistance increased obviously, and the corresponding SERN performance is dramatically dropped. Furthermore, the flow separation under this over-expanded condition can lead to large nose-up pitching moment, which brings out the additional difficulty for the aircraft control (Christopher and Jaime, 1991). The problem of hypersonic vehicle in the transonic region is an imperative key technology to be solved for the designer, and how to effectively improve the performance of SERN under over-expanded condition has become an important issue in the integrated design of hypersonic propulsion system. (Lynn and Daric, 2004).

Under NPR condition, the SERN performance deterioration is closely related to the flow separation size and the separation starting position on the upper expansion ramp (Yu *et al.*, 2014). In order to keep high performance in a wide flight envelope, control of the internal flow separation and the separation starting position are necessary for SERN. Mechanical adjustment method (Karen and Scott, 1996; Lederer, 1996; Hao and Wang, 2009), secondary flow injection method (Grønland and Berens, 1995; Thomas, 1995; Grønland *et al.*, 1997), external burn method (Yungster, 1994) and air ejector (Yang, 2009) were used to improve SERN flow quality and performance under over-expanded condition, but these methods all increased the weight and the structure complexity of the exhaust system, also brought out additional cooling problems. With the development of the flow control technology, the passive flow control technique had attracted concerns of researchers to perform massive investigations due to its simple and reliable property. Among them, the passive cavity flow control technique, which derived from supercritical wings design (Scott *et al.*, 1996). It had been proved that the passive cavity flow control technique had the capacity of controlling flow separation and decreasing noise (Bae and Moon, 2009). In the experimental study of Bauer and Hensch (1992), the passive cavity was joined to the fore-body of the missile, results showed that the passive cavity could eliminate the asymmetrical load distribution on the axisymmetric fore-body under the high attack angle condition. Yaga *et al.* (2003) successfully adopted

the passive cavity to strengthen the flow mixing and reduce losses. Kraushaar and Chokani (1997) used the passive cavity to reduce the aft-body drag of the nozzle. In addition, some researchers had introduced the passive cavity into the asymmetrical nozzle (Scott *et al.*, 1996; Elmiligui *et al.*, 2005), and made a preliminary study on this passive flow control method. Results showed the passive cavity could effectively suppress the separation flow, and reduce the installation drag of the nozzle. Jürgen and Alfred (1999) began to concern the usage of the passive cavity in the SERN, in which the 1/100 scaled SERN model of ELAC aircraft were studied, the potential advantage of the passive cavity and the flowfield of the SERN were analyzed. It was found that the SERN thrust vector could reduce 30 % as when the passive cavity control method was adopted. But the application range of the passive cavity control method was not mentioned, and the flow control mechanism of the passive cavity was lack of consideration.

The passive cavity is introduced to improve the SERN performance under over-expanded condition, and the two-dimensional flowfield of SERN with and without passive cavity had been compared in the former research (Zhou *et al.*, 2015), the influence of the passive cavity on the flow pattern of the two-dimensional SERN has been shown. In this paper, for the sake of considering the three-dimensional flow effect caused by the SERN side wall and deeply explore the flow control mechanism of the passive cavity, numerical simulation is conducted for the three-dimensional SERN with passive cavity adopted, the effective NPR range that the passive cavity can improve SERN performance is discussed, and the effects of passive cavity geometric parameters on the three-dimensional flow structure and the performance of the SERN are studied.

2. NUMERICAL SIMULATION METHODOLOGY AND MODEL

2.1 Simulation Method

The three-dimensional flowfield in SERN are carried out by FLUENT software. Fully 3D, steady, compressible, Reynolds averaged Navier-Stokes equations are solved. The equations were discretized in finite volume form, with the second order resolution option used in the advection scheme, and two-equation standard k- ϵ turbulence model was chosen according to the result of Yang (2009) on SERN.

2.2 Calculation Model

The interior flow of the baseline SERN is rectangular channel, making the middle section of the nozzle ($Z=0$) as the center plane of symmetry. A half part of SERN model is shown in Fig. 1. On the center symmetry plane, the point which is located at the lower wall of the nozzle throat is defined as the origin of coordinates. The aspect ratio at the nozzle throat is 4.63. The SERN throat height is 0.511m. The axial length of the upper expansion ramp is

19.57m, the flap length is 1.01m, and the height of the SERN outlet is 3.743m. The connection of the trailing edge of cowl to the trailing edge of upper expansion ramp is the side wall of SERN.

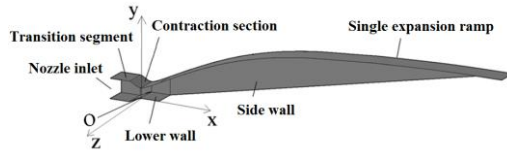
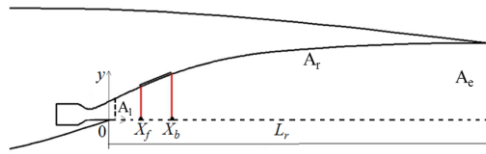
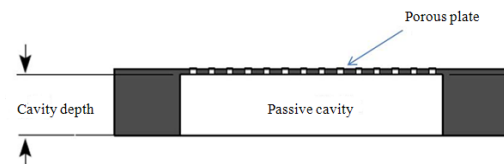


Fig. 1. Sketch of the baseline SERN.

For the SERN with passive cavity applied, as shown in Fig. 2, the modification design is performed on the upper wall configuration of the baseline SERN. The modified upper wall consists of three parts, which are baseline upper wall, porous plate and cavity body respectively. Among them, the porous plate covers on the passive cavity body to form the passive cavity configuration, and then this passive cavity structure is embed in the nozzle basal body of the SERN. The leading edge of the passive cavity is marked as X_f , and the trailing edge labeled as X_b . L_r is the axial length of the upper expansion ramp. When the position of the passive cavity structure is changed, the arc length from X_f to X_b keeps as a constant value, moving the passive cavity along the ramp. Parameters of the baseline passive cavity structure are defined as follows: X_f/L_r is 8.11 %, X_b/L_r 16.22 %, the percent of porosity is 9.16 %, and the cavity depth is 95 millimeters.



(a) SERN configuration

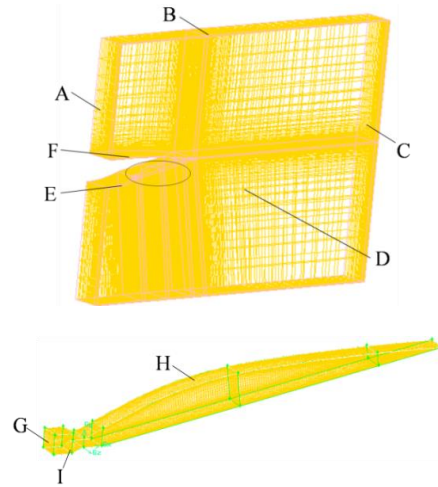


(b) geometry of passive cavity

Fig. 2. Sketch of SERN with passive cavity.

The computational mesh is shown in Fig. 3. Due to the symmetrical feature of SERN along Z direction, half of the nozzle configuration and far field are chosen as the computational domain to reduce the calculation cost. The computational domain includes the SERN internal flow field and an external domain to consider the interaction between the SERN and the hypersonic aircraft. The extend magnitude of the external domain is referred to the nozzle throat height H , in which about $120H$ downstream the nozzle outlet, $15H$ beneath the sidewall (along Z direction), and $60H$ normal to the nozzle axis (Y direction). Structured and

unstructured grids are coupled, and grid near the nozzle wall are fined. The mesh number with 3,217,508 elements is used after grid independent analysis in the paper.



A, B, J: Pressure-far-field; C: Pressure-outlet; D: Symmetry; E, F, H, I: Wall; G: Pressure-inlet

Fig. 3. Computational mesh of SERN.

Pressure inlet boundary with uniform total pressure, total temperature and flow angle is applied at SERN inlet. Pressure far field boundary conditions are specified for the external flow boundary, of which static pressure, Mach number and flow direction are prescribed. Static pressure is specified at the far field outlet. Non-slip adiabatic wall boundary conditions are applied on all solid walls of SERN and the cavity body. It shows in Fig. 2(b) that porous holes are arranged on the porous plate of the passive cavity, the flow can either enter or blow out from the porous holes of the porous plate, and the no-slip, non-penetration and adiabatic wall boundary condition is adopted on porous plate wall. On the center symmetry plane, symmetry boundary condition is specified according to its symmetric configuration character.

2.3 Performance Parameter of SERN

Axial thrust coefficient $C_{f_{gx}}$ is used to estimate the SERN performance, with the definition as:

$$c_{f_{gx}} = F_j / F_i$$

The actual axial thrust F_j is defined as follows:

$$F_j = \int_{A_l} \rho V_x^2 dA + \int_{A_l} (P - P_\infty) dA + \int_{A_r} (P - P_\infty) dA_x - X_{fx}$$

where $\int_{A_l} \rho V_x^2 dA$ and $\int_{A_l} (P - P_\infty) dA$ are the axial

thrusts produced by the momentum and the pressure differential on A_l surface respectively.

$\int_{A_r} (P - P_\infty) dA_x$ is the axial thrust contributed by

the pressure distribution on A_r surface. The last term X_{fx} is the axial component of the friction force on A_r surface.

F_i is expressed as:

$$F_i = W_p \sqrt{RT_j} [2\gamma / (\gamma - 1)] \left[1 - (P_\infty / P_j)^{(\gamma-1)/\gamma} \right]$$

3. RESULT AND DISCUSSION

3.1 Validation of the Numerical Method

The SERN model (Capone *et al.*, 1992) was simulated and compared with the experimental data to validate the numerical method adopted. The distribution of the axial thrust coefficient is presented in Fig. 4 under different NPR with Ma of 0, it shows good agreement is achieved in most positions; and the deviation between them is less than 1 percent. Therefore, the equation discretization, turbulence model and solution algorithm selected in this paper can reasonably predict the flow field in the SERN.

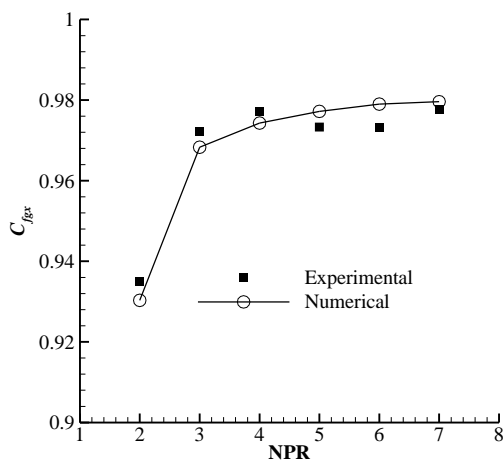


Fig. 4. Distribution of the axial thrust coefficient under different NPR (Ma=0).

3.2 NPR Range of the Passive Cavity Application on SERN

In order to obtain the effective NPR range for the passive cavity SERN, the simulation was performed for the passive cavity SERN from NPR of 5 to 10, where the external flow Mach number is specified as 0.5.

The flowfield of the SERN with and without passive cavity was compared firstly under NPR of 5. Mach number distributions on the symmetry plane are displayed in Fig. 5, and pressure distribution on the upper expansion ramp is presented in Fig. 6. For the baseline SERN in Fig. 5(a), an oblique shock is generated at the inner flow outlet of the nozzle, and then propagates downstream. The boundary layer separation is induced when the shock intersects with the expansion ramp, and an induced shock is formed before the separation flow zone of the boundary layer, thus, the corresponding static pressure abruptly rises. A reattached shock is generated behind the separation zone as the flow deviates from the upper expansion ramp, resulting in a further pressure increase. Shock train phenomenon

appears in the SERN as the restricted shock separation is produced under these NPR, and then the shock is reflected multiply on the upper expansion ramp, leading to repeated abruptly rise in pressure, as shown in Fig. 6.

As described above, $\int_{A_r} (P - P_\infty) dA_x$ (axial thrust

produced by pressure differential on the upper expansion ramp) is one of the components of axial thrust. For the passive cavity SERN in Fig. 6, the first two pressure peaks are both significantly higher than the corresponding pressure of the baseline SERN at the plane of $Z=0$ and $Z=0.2$, thus the static pressure integral along the upper expansion ramp is relatively larger for passive cavity SERN. Therefore, the axial thrust coefficient is increased and the SERN performance is improved with the application of the passive cavity.

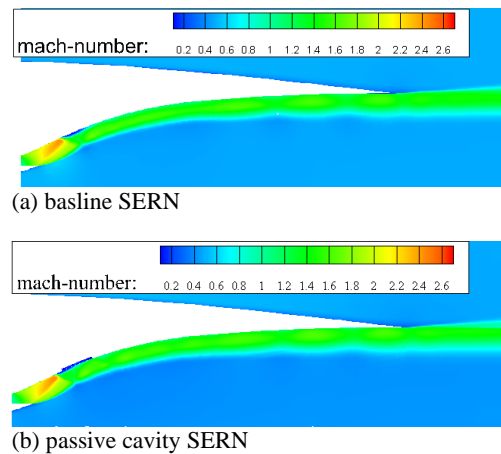
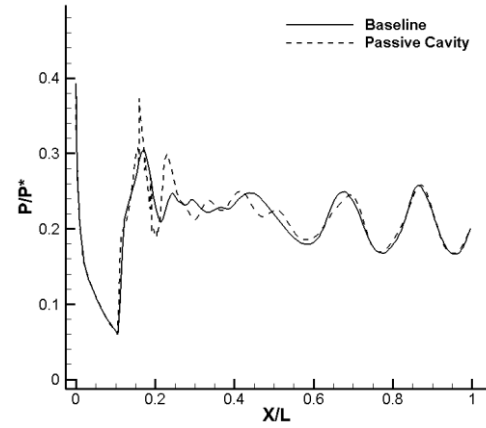


Fig. 5. Mach number distributions of the SERN symmetry plane (NPR=5).

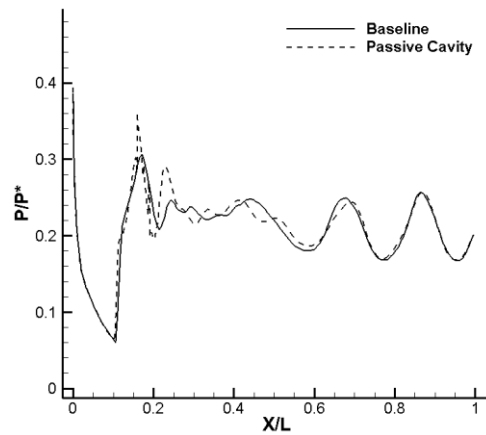
Figure 7 gives Mach number distributions on the symmetry plane under different NPR. Stable reverse flow zone all occurs under different NPR condition. With the increase of NPR, the oblique shock generating at the inner flow outlet of the nozzle is gradually pushed out. The shock angle becomes smaller; the induced shock is also gradually away from the nozzle throat. Consequently, the separation zone moves backward and becomes larger; the pressure distribution on the upper expansion ramp changes with the variety of NPR. And in the calculated pressure ratio range, passive cavity structure affects the pressure distribution of the nozzle through its pressure adjustment which determines by the pressure difference before and after the induced shock, and then has an impact on the nozzle thrust coefficient.

Upper expansion ramp pressure distributions under different Z planes are displayed in Fig. 8. Here, the axial position of at the inner flow outlet of the nozzle is defined as the starting point of the abscissa, and the abscissa is non-dimensional-normalized by the axial extension length of the upper expansion ramp L_r . It shows that obvious three-dimensional flow effect exists on the pressure

distributions at different Z sections. As compared with the distribution on the symmetry plane, the pressure magnitude at the first peak decreases on the Z section which is far away from the central symmetry plane. On each Z section, repeated abruptly rise in pressure due to the reflection of the shock trains.



(a) Z=0



(b) Z=0.2

Fig. 6. Upper expansion ramp pressure distributions of Z planes (NPR=5).

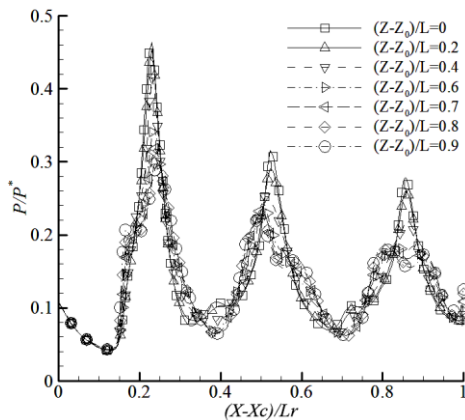
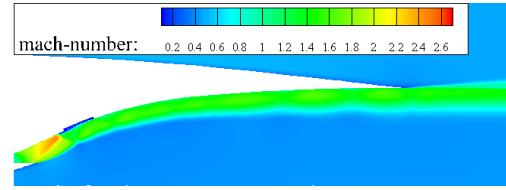
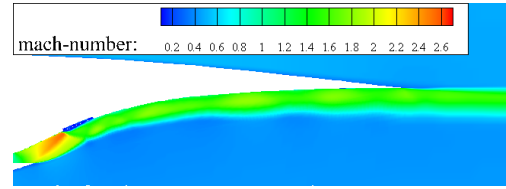


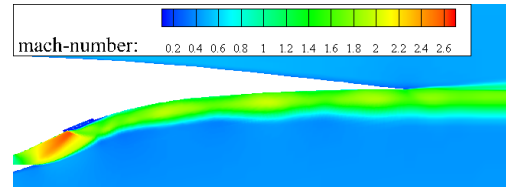
Fig. 8. Upper expansion ramp pressure distributions of Z planes (NPR=7) (percent of porosity=9.16 %, aperture=40 mm, cavity depth=95 mm, cavity position =8.11% Lr).



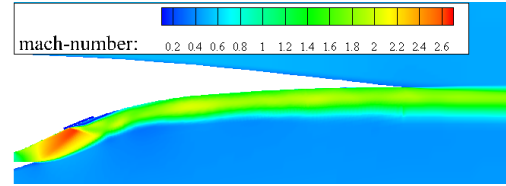
(a) NPR=5



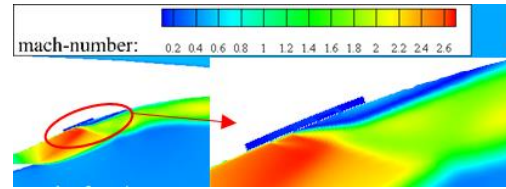
(b) NPR=6



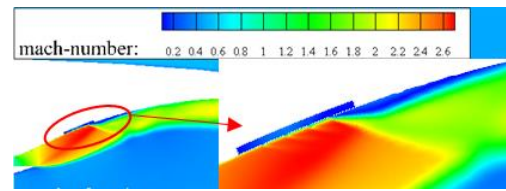
(c) NPR=7



(d) NPR=8



(e) NPR=9



(f) NPR=10

Fig. 7. Mach number distributions of the SERN symmetry plane under different NPR (percent of porosity=9.16 %, aperture=40 mm, cavity depth=95 mm, cavity position =8.11% Lr).

The SERN performance under different NPR is shown in Table 1. Due to the pressure adjustment of the passive cavity structure, further increase for pressure all exist for different NPR, and multiple pressure rises occur as usual under the reflection effect of shock trains. The position occurring the abrupt pressure rise shifts downstream with the increase of NPR, as the reason that the shock wave is gradually pushed afterward. Pressure differential on the upper expansion ramp is known as an

Table 1 Improvement effectiveness of the axial thrust coefficient of SERN

	NPR					
	5.00	6.00	7.00	8.00	9.00	10.00
$C_{f_{gx}}$ - passive cavity	0.6164	0.6883	0.7358	0.7685	0.7933	0.8097
$C_{f_{gx}}$ -baseline	0.5977	0.6707	0.7153	0.7566	0.7879	0.8065
$\Delta C_{f_{gx}}$ (%)	3.13	2.63	2.87	1.57	0.69	0.40

important factor to determine the axial thrust. As this case, the pressure integrals is increased for passive cavity SERN due to the increased pressure peak, which is produced by the pressure adjustment of the passive cavity. Thus, compared with the baseline SERN, the axial thrust coefficient is increased correspondingly.

In the calculated NPR range which is from 5 to 10, the SERN performances are all improved with the application of the passive cavity. Under the lowest NPR of 5, the flow is severely over-expanded, the thrust coefficient is much lower than that it has under other NPR, the flow control effectiveness is more obvious, and the maximum enhancement can achieve 3.13 %. As described in the above analysis, passive cavity structure affects the pressure distribution of the nozzle through the pressure adjustment, the improvement effectiveness of the axial thrust coefficient is related to the shock wave position and the separation zone position. From the pressure distribution of SERN in Fig. 7, it shows the passive cavity almost covers the whole separation zone under the case that NPR is 6, the reverse flow is confined in the passive cavity, the pressure adjustment of the passive cavity is not obvious due to the little pressure difference in the reverse flow, thus, the improvement effectiveness of the axial thrust coefficient under NPR of 6 is smaller than that it has under NPR of 7, as the pressure adjustment of the passive cavity is relatively obvious due to the pressure difference before and after the shock.

3.3 SERN with Different Parameters of Passive Cavity

From the structure characteristics of the passive cavity, shown in Fig. 2, it can be seen that several geometric parameters are involved to describe the passive cavity, which includes the cavity position, percent of porosity, aperture and depth of cavity. Thus the effect of these geometric design parameters on SERN performance are discussed, to explore the flow mechanism in passive cavity SERN, and provide the support for the passive cavity design which can effectively improve SERN thrust coefficient under over-expanded condition.

3.3.1 Position of Passive Cavity

Position of the passive cavity is firstly investigated. Here, the baseline geometric parameters of passive cavity structure are specified as follows: the percent of porosity is 9.16 %, the cavity depth is 95 mm, and the aperture is 40 mm. The flow field is simulated under the condition that the outer flow

Mach number is 0.5 and NPR is 7. The position of the passive cavity is characterized by the leading edge of the passive cavity X_p/L_r .

Figure 9 presents Mach number distributions at the symmetry plane. For the passive cavity SERN, the passive cavity builds a bridge for the flow before and after the shock, the pressure difference before and after the shock motivates the low-velocity flow behind the shock to enter into the cavity and discharge from the holes before the shock. Due to the pressure adjustment effect of the passive cavity, the local flow is altered near the induced shock root, resulting in the change of the pressure distribution and the intensity of the induced shock. When the position of the passive cavity is moved downstream, the cavity position is not located near the induced shock, and the passive cavity mainly impacts on the boundary layer separation which is caused by intersection of the oblique shock with the upper expansion ramp. Since the pressure behind the induced shock is larger than that in the core flow, the inverse flow is motivated to enter into the cavity body from the first holes, and discharge from the back holes on the porous plate of the cavity, then goes ahead close to the upper ramp wall. The inverse flow zone would be suppressed correspondingly by the cavity due to the flow adjustment effect in the passive cavity. When the passive cavity position is located at X_p/L_r of 16%, the inverse flow is completely motivated to enter into the cavity, and guided by the cavity to mix with the core flow, no separation occurs at this case. After that, the passive cavity position moves toward the nozzle exit continually, the distance between the passive cavity and the induced shock increases correspondingly, the cavity does not touch the separation flow zone which is behind the induced shock, the cavity only can influence the flow around the cavity, the pressure regulation effect of the cavity is limited, the passive cavity does not adjust the intensity of the induced shock and suppress the zone of the separation flow any more. Now, the induced shock is produced at the location around 8% L_r , and flow separation appears behind the induced shock, which is similar to the flow in the baseline SERN as shown in Fig. 5.

The SERN thrust coefficients are displayed in Fig. 10 under different passive cavity position, and the performance improvement of the passive cavity SERN are showed in Table 2. When the passive cavity position is located at 3.9 % L_r , the intensity of the induced shock is altered due to the pressure adjustment effect of the passive cavity, a stable separation zone is formed, the function of the

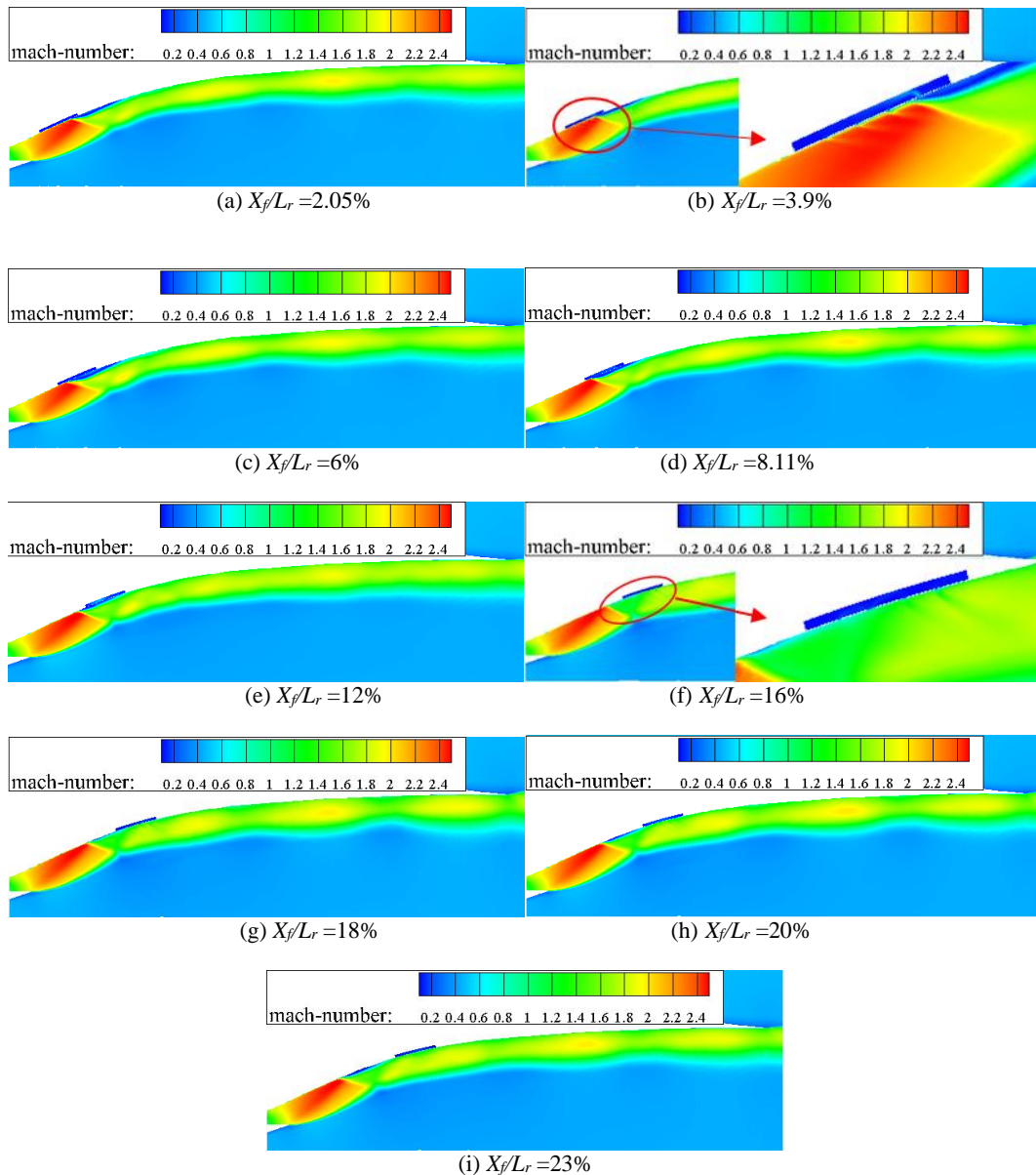


Fig. 9. Mach number distribution at SERN symmetry plane under different cavity position (percent of porosity=9.16 %, aperture=40 mm, cavity depth=95 mm).

passive cavity can be expressed as a regulator of the induced shock intensity at this case, and the thrust coefficient can be improved up to 3.39 %. With the movement of the cavity downstream, the passive cavity is apart from the induced shock, the adjustment effect of the passive cavity on the flow structure near the induced shock is weakened, that is the effect of the passive cavity whose function is a regulator of the induced shock intensity becomes smaller. When the position of the passive cavity is located at 12 % L_r , the width of the passive cavity covers the whole separation flow zone, the pressure difference among the porous holes of the passive cavity is very small, the passive cavity has not enough potential to drive the low-velocity flow behind the shock to enter into the cavity and alter the intensity of the induced shock. Thus, the pressure adjustment effectiveness by the passive cavity achieves a low value as the passive cavity

position is moved from 8.11% L_r to 12% L_r . When the position of the passive cavity is moved downstream further, the passive cavity begins to adjust the inverse flow which is behind the induced shock, and suppress the zone of this separation flow. When the position of the passive cavity is located at 16 % L_r , the separation zone is vanished, the function of passive cavity can be expressed as a separation restrainer, and the axial thrust coefficient improves 2.49 %. When the passive cavity moves to the exit of nozzle, although the pressure adjustment of the passive cavity is limited due to the larger distance between the induced shock and the passive cavity, the flow separation still appears, and the flow pattern is similar to the one in the baseline SERN, the SERN performance cannot get an obvious improvement using passive cavity control method.

Table 2 Improvement effectiveness of the axial thrust coefficients of SERN under different cavity position

	X_f/L_r							
	3.9%	6%	8.11%	12%	16%	18%	20%	23%
$\Delta C_{f_{gx}}$ (%)	3.39	2.84	2.87	1.00	2.49	1.88	1.80	1.55

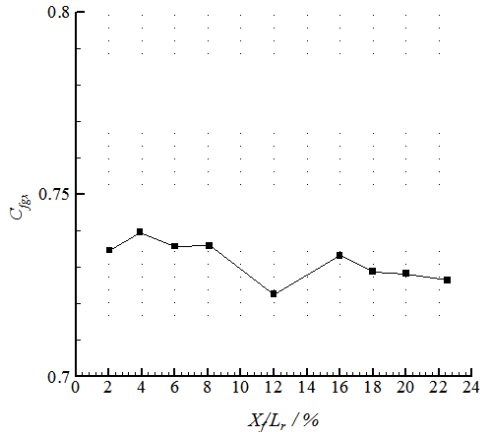


Fig. 10. Axial thrust coefficient of the passive cavity SERN under different cavity position (percent of porosity=9.16 %, aperture=40 mm, cavity depth=95 mm).

From analysis mentioned above, it can be found that the passive cavity has the functions of regulating the induced shock intensity or restraining flow separation, the reason for the change in its function is related to the relative location between the induced shock and the passive cavity position. Two optimum passive cavity positions exist for the passive cavity SERN to get the improved performance, which is dominated by the function of the passive cavity. When the passive cavity acts as a regulator of the induced shock intensity, the intensity of the induced shock is altered, and the loss caused by the shock wave is decreased consequently. When the passive cavity acts as a separation restrainer, the separation zone is suppressed, and the corresponding loss induced by the inverse flow is also reduced. No matter what is the function of the passive cavity, the influence of the passive cavity reflects on the pressure integral along the upper expansion ramp. And when the intensity of the induced shock is altered, the pressure integral of the upper expansion ramp is higher than the one when the flow separation is restrained. Then, the performance improvement effectiveness when the passive cavity acts as a regulator of the induced shock intensity is better than the case when passive cavity acts as a separation restrainer.

3.3.2 Percent of Porosity

The effect of percent of porosity (proportion of porous holes area to porous plate area) is also investigated, where percent of porosity are 9.16 %, 13.74 %, 18.32 %, 22.90 %, and 27.48 % respectively. The aperture of porous plate, the passive cavity depth and the passive cavity position keep as 40 mm, 95 mm and 8.11%, Ma is 0.5 and

NPR are 5, 6, 7 respectively.

Figure 11 gives the pressure distribution on the passive cavity bottom, where NPR is selected as 7, and the horizontal ordinate is non-dimensional by the length of the passive cavity. The low-velocity flow behind the shock is motivated to enter the cavity as the pressure differential exists before and after the shock, and discharge from the first hole before the shock, then the induced shock is pushed and its intensity is changed correspondingly. More porous holes on the porous plate exists with the increasing percent of porosity, making the first hole to be closer to the cavity edge. Thus, the starting position of the flow separation shifts forward under the larger percent of porosity, the inverse flow and the mass flow rate entering / discharging from the cavity increases with the increment in percent of porosity. Since more fluid is discharged from the cavity from post-shock to pre-shock, the boundary layer zone of the shock expands upstream, the pressure displays the progressive increase distribution, and then the corresponding intensity of the induced shock would be gradually weakened, inducing the pressure distribution with lower magnitude. The separation flow zone also enlarges with the increase of the percent of porosity, reduces the pressure magnitude on the passive cavity bottom wall, and then impacts on the pressure of the upper expansion ramp, inducing the lower growth of the pressure integral. Therefore, the performance improvement effectiveness of passive cavity SERN reduces when the percent of porosity increases, as shown in Fig. 12.

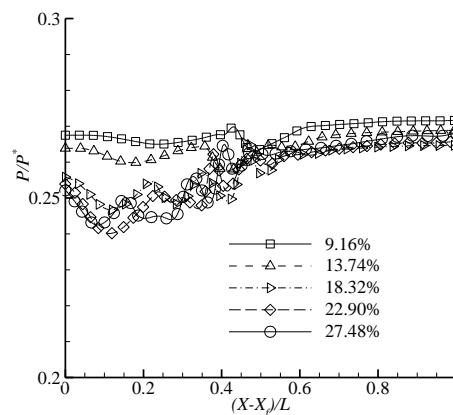


Fig. 11. Bottom pressure distributions of passive cavity under different percent of porosity (aperture=40 mm, cavity depth=95 mm, cavity position =8.11% L_r).

From the analysis described above, it shows the passive cavity can effectively improve the SERN performance by increasing the pressure magnitude

on the upper expansion ramp. The axial thrust coefficient of passive cavity SERN is presented in Fig. 12, with different percent of porosity and NPR adopted. By adjusting the flow separation size in the passive cavity body and the mass flow rate entering / discharging from the cavity, the passive cavity can change the pressure distribution and the intensity of the induced shock, the SERN performance are all improved under these cases, and the larger the percent of porosity is, the smaller gain in the axial thrust. The performance enhancement is more obvious under lower NPR condition, which is similar as the result in Table 1. Moreover, the passive cavity SERN has the different suitable NPR condition, which is related to the intensity of the induced shock and the inverse flow zone. Under different NPR conditions, the passive cavity SERN can obtain the best performance when percent of porosity is 9.16 %.

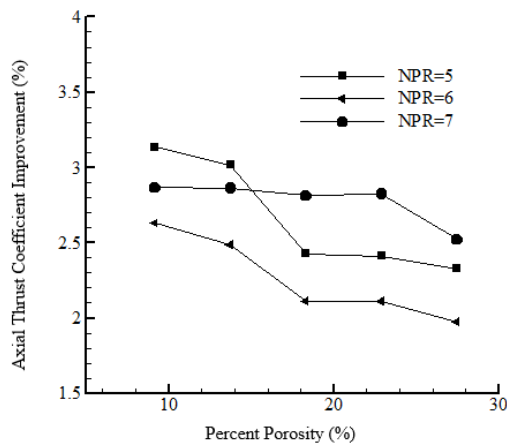


Fig. 12. Axial thrust coefficient of passive cavity SERN under different percent of porosity (aperture=40 mm, cavity depth=95 mm, cavity position =8.11% L_r).

3.3.3 Aperture Size

Figure 2(b) shows that the porous plate covers on the passive cavity body to form the passive cavity configuration. Porous holes are arranged on the porous plate of the passive cavity, and the flow can either enter in or discharge from the porous holes. The impact of the porous plate on the flow through the passive cavity can reflect on its geometric parameters, which are percent of porosity and aperture size of the porous holes, therefore, the influence of aperture size is also investigated under a certain percent of porosity. As percent of porosity is proportion of porous holes area to porous plate area, the porous hole number reduces when the apertures increases, while the relative position of the first porous hole row to the cavity edge does not alter obviously, and the aperture changes from 20 mm to 53 mm. The calculation are performed under the same condition of percent of porosity, cavity depth, cavity position, Ma number and NPR, which are 9.16%, 95 mm, 8.11%, 0.5 and 7 respectively.

Figure 13 displays Mach number distribution on the symmetry plane. A stable separation flow is formed close to the passive cavity. The flow pattern of

passive cavity SERN changes a little with the increase of the aperture, the size and the starting position of the flow separation almost remains same.

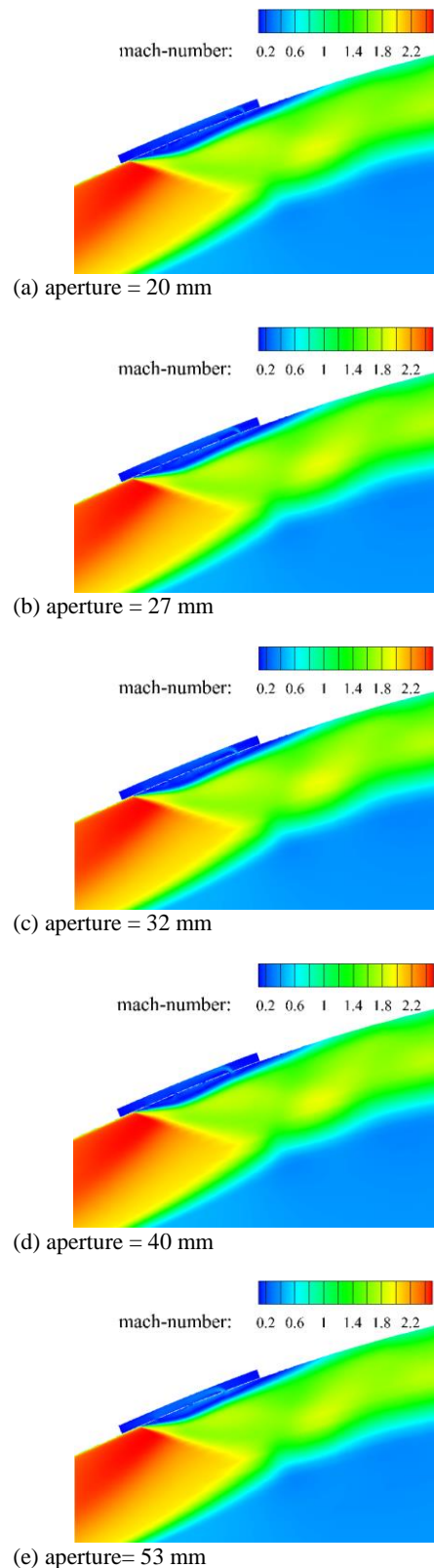


Fig. 13. Mach number distributions of passive cavity SERN under different aperture (percent of porosity=9.16 %, cavity depth=95 mm, cavity position =8.11% L_r).

Besides, the high-pressure zone, abrupt pressure rising position and pressure peak value all nearly keep same under these aperture, as shown in Fig. 14. The shock position, shock intensity and shock angle of the induced shock are almost same. Moreover, the shock trains also remain unchanged. Flow separation generally appears at the first row of porous hole plate under these cases. As the position of the first porous hole row relative to the cavity edge does not change obviously at these cases, and the percent of porosity are same, the mass flow rates that entering / discharging from the passive cavity body are nearly. Thus, the intensity of the induced shock almost keeps constant, as well as the pressure distribution is. Therefore, the pressure characteristic in the SERN changes a little under these apertures, and the performance of passive cavity SERN almost coincides. Thus, the aperture is insensitive to the flowfield in the SERN, and the aperture size is not crucial in the design process.

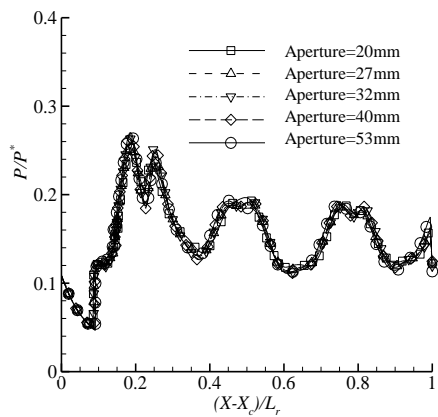


Fig. 14. Pressure distributions on upper expansion ramp under different aperture of cavity (percent of porosity=9.16 %, cavity depth=95 mm, cavity position =8.11% L_r).

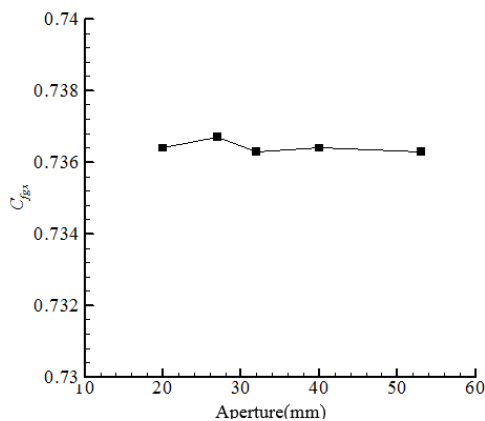


Fig. 15. Axial thrust coefficient of passive cavity SERN under different aperture (percent of porosity=9.16 %,cavity depth=95 mm, cavity position =8.11% L_r).

3.3.4 Cavity Depth

Then, the investigation on the effect of the cavity depth on SERN performance is carried out. Five cavity depths are chosen. The calculations are performed under the same condition of percent of

porosity, cavity position, aperture size, Ma number and NPR, which are 9.16%, 40 mm, 8.11%, 0.5 and 7 respectively.

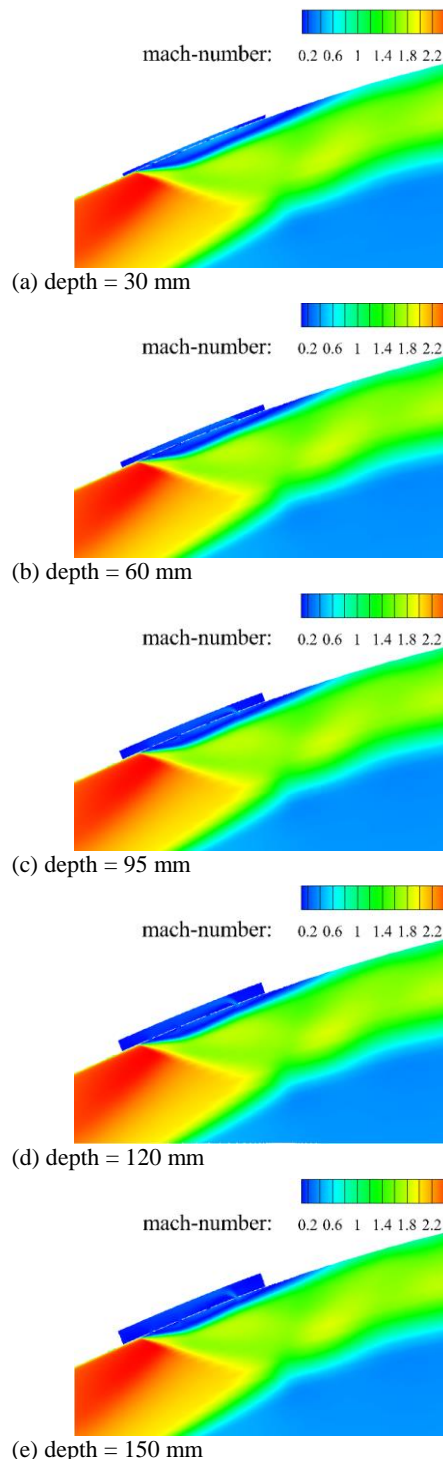


Fig. 16. Mach number distributions of passive cavity SERN under different cavity depth (percent of porosity=9.16 %, aperture=40 mm, cavity position =8.11% L_r).

Figure 16 presents Mach number distribution on the symmetry plane. Under different cavity depth conditions, the flow characteristic of passive cavity SERN alters little, the size and the starting position of the flow separation almost maintain same.

As the same aperture and percent of porosity are adopted for the calculation under different cavity depth, the flow enters / discharges from the same position of the passive cavity with the same mass flow rate, resulting in the same effect on the flow close to the root of the induced shock. In Fig. 17, pressure on the upper expansion ramp almost coincides with the change of cavity depth. Thrust coefficient changes slightly under different cavity depth, as shown in Fig. 18.

In summary, the passive cavity structure has the function to regulate the induced shock intensity or restrain flow separation, either of these two functions can effectively improve the flow quality and performance of the SERN. Among the cavity geometric parameters, percent of porosity can significantly impact on the flowfield in the SERN as compared with other cavity parameters.

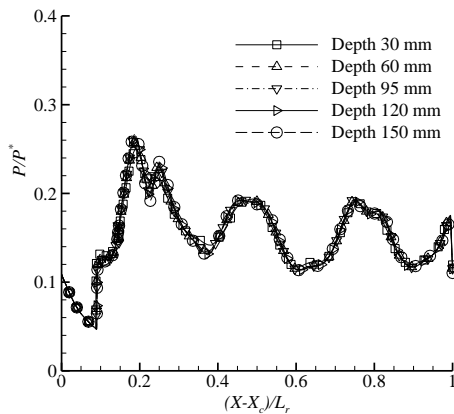


Fig. 17. Pressure distribution on upper expansion ramp of passive cavity SERN under different cavity depth (percent of porosity=9.16 %, aperture=40 mm, cavity position =8.11% L_r).

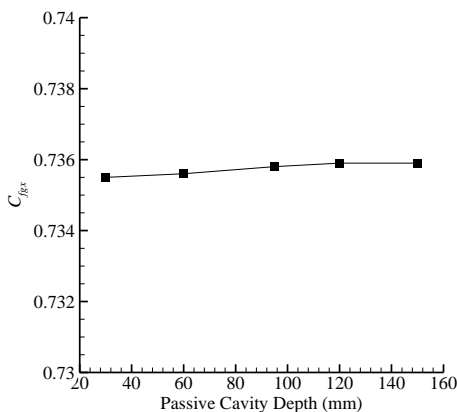


Fig. 18. Axial thrust coefficient of passive cavity SERN under different cavity depth (percent of porosity=9.16 %, aperture=40 mm, cavity position =8.11% L_r).

4. CONCLUSIONS

The three-dimensional flowfield in the SERN are numerically investigated under the over-expanded condition, and the impact of passive cavity on the SERN is discussed, main conclusions are as

follows:

- 1) The passive cavity can alter the intensity of the induced shock by using the pressure differential before and after the shock, and then increase the local pressure on the upper expansion ramp. The passive cavity structure is valuable to the axial thrust coefficient, and the maximum improvement of SERN performance can achieve 3.13 %.
- 2) Among the cavity geometric parameters, percent of porosity is a key parameter to impact SERN performance, and the improvement effectiveness of the SERN performance reduces with the increasing percent of porosity. While cavity depth and aperture size are insensitive to the SERN performance.
- 3) The passive cavity has the function of regulating the induced shock intensity or restraining flow separation under different passive cavity position, the reason for the change in its function is dominated by the relative position between the induced shock and the position of the passive cavity. Two optimum positions exist for the passive cavity to improve the SERN performance as much as possible, which is dependent on the detailed function of the passive cavity.

The experimental investigation the SERN under over-expanded condition would be performed in the future, concerning the flow control effectiveness of the passive cavity under different conditions. Further flowfield analysis would be carried out for the passive cavity SERN to obtain the design principle of passive cavity.

ACKNOWLEDGEMENTS

This work was supported by National Natural Science Foundation of China (No. 51876176 and No. 51576163) and the financial support of MIIT.

REFERENCES

- Bae, Y., J. Ye and Y. Moon (2009). Effect of porous surface on the flat plate self-noise. *15th AIAA/CEAS Aeroacoustics Conference*. 11-13 May, Miami, Florida, United States, AIAA-2009-3311.
- Bauer, S. X. S. and M. J. Hemsch (1992). Alleviation of side force on tangent-ogive forebodies using passive porosity. *Journal of Aircraft* 31(2), 354-361.
- Capone, F. J., R. J. Re and E. A. Bare (1992). Parametric Investigation of single-expansion-ramp nozzles at Mach numbers from 0.60 to 1.20. *NASA TP-3240*
- Christopher, A. S. and J. M. Jaime (1991). The design and performance estimates for the propulsion module for the booster of a TSTO vehicle. *Aircraft Design Systems and Operations Meeting*, 23-25 September 1991, Baltimore, MD, United States, AIAA-1991-

- 3136.
- Deere, K. A. and S. C. Asbury (1999). Experimental and computational investigation of a translating-throat single expansion ramp nozzle. *NASA/TP*, 1999-209138.
- Elmiligui, A., K. Abdol-Hamid and C. Hunter (2005). Numerical investigation of flow in an over-expanded nozzle with porous surfaces. *33rd AIAA Fluid Dynamics Conference and Exhibit*. 23-26 June, Orlando, Florida, United States, AIAA-2005-4159.
- Granland, T. and T. Berens (1995). Nozzle / afterbody integration for hypersonic vehicles by means of secondary air injection. *AIAA 6th International Aerospace Planes and Hypersonics Technologies Conference*. 3-7 April, Chattanooga, TN, United States, AIAA-1995-6050.
- Gronland, T. A., J. L. Gambier and S. Wallin (1997). Nozzle / afterbody performance for hypersonic airbreathing vehicles. *33rd AIAA/ASME/SAE/ASEE Joint Propulsion Conference & Exhibit*. 6-9 July, Seattle, WA, AIAA-1997-3166.
- Hao, D. X. and Z. X. Wang (2009). The design and flow field simulation of single expansion ramp nozzle with variable flaps. *Machinery Design and Manufacture* 12, 8-10.
- Jürgen, G. and E. B. Alfred (1999). Enhance thrust-efficiency of over-expanded nozzles by passive venting. *Mechanics of Passive and Active Flow Control* 69-74.
- Karen, A. D. and C. A. Scott (1996). An experimental and computational investigation of a translating throat single expansion-ramp nozzle. *32nd AIAA/ASME/SAE/ASEE Joint Propulsion Conference and Exhibit*. 1-3 July, Lake Buena Vista, FL, United States, AIAA-1996-2540.
- Kraushaar, S. and N. Chokani (1997). Afterbody separation control using passive porosity. *33rd AIAA/ASME/SAE/ASEE Joint Propulsion Conference and Exhibit*. July 6-9, Seattle, WA, United States, AIAA-1997-3003.
- Lederer, R. (1996). Testing the actively cooled fully variable hypersonic demonstrator nozzle. *7th Space Plane and Hypersonic Systems and Technology Conference*. 18-22 November, Norfolk, VA, United States, AIAA-1996-4550.
- Lynn, E. S. and W. E. Daric (2004). Turbine based combination cycle (TBCC) propulsion subsystem integration. *40th AIAA/ASME/SAE/ASEE Joint Propulsion Conference and Exhibit*, 11-14 July 2004, Fort Lauderdale, Florida, AIAA-2004-3649.
- Scott, C. A., L. G. Christopher and A. H. Craig (1996). A passive cavity concept for improving the off-design performance of fixed-geometry exhaust nozzles. *32nd AIAA/ASME/SAE/ASEE Joint Propulsion Conference and Exhibit*. 1-3 July, Buena Vista, FL, United States, AIAA-1996-2541
- Thomas, M. B. (1995). Experimental and numerical analysis of a two-duct nozzle / afterbody model at supersonic mach numbers. *AIAA 6th International Aerospace Planes and Hypersonics Technologies Conference*. 3-7 April, Chattanooga, TN, United States, AIAA-1995-6085.
- Yaga, M., S. Tabata, P. Doerffer and K. Oyakawa (2003). Numerical simulation of supersonic mixing enhancement with porous cavity. *33rd AIAA Fluid Dynamics Conference and Exhibit*. 23-26 June, Orlando, Florida, United States, AIAA-2003-3461.
- Yang, C. Y. (2009). Numerical investigation on pneumatic performances and infrared radiation characteristics of an S-shaped tunnel single expansion ramp nozzle (Master Dissertation). *Nanjing University of Aeronautics and Astronautics*, Nanjing, China.
- Yu, Y., J. L. Xu, J. W. Mo and M. T. Wang (2014). Principal parameters in flow separation patterns of over-expanded single expansion ramp nozzle. *Engineering Applications of Computational Fluid Mechanics* 8(2), 274-288.
- Yungster, S. and C. Trefny (1994). Computational study of single-expansion-ramp nozzles with external burning. *32nd Aerospace Sciences Meeting and Exhibit*, 10-13 January, Reno, NV, United States, AIAA-1994-0024.
- Zhou, L., H. Xiao and Z. X. Wang (2015). Effect of passive cavity on high pressure ratio single expansion ramp nozzle. *Journal of Aerospace Power* 30(8), 1811-1817.